Nano-assemblies for biomedical applications based on Prussian blue Nanoparticles

Erasmus Mundus Joint Master Degree in Surface, Electro, Radiation, & Photo Chemistry (SERP+)

By

Andrea Merlo

Supervisors:

Laure Catala

Professeur

Riya George

PhD

ICMMO - ECI

This page was intentionally left blank

Table of contents

ABSTRACT

Cancer is one of humankind's most feared diseases today, and many methods have been conceived to treat and image it. In this context, Prussian Blue (PB) can be used in the simultaneous application of several techniques to obtain a stable and biocompatible theranostic agent with extremely useful and interesting properties. Its porous and electrically charged structure makes it a possible carrier for drug delivery; its ability to absorb near-infrared radiation (NIR) makes it as an agent for photothermal treatments (PTT). At the same time, PB is also an excellent contrast agent for various imaging techniques, such as photoacoustic imaging (PAI) or nuclear magnetic resonance imaging (MRI), which can be used at the same time in a dual way.

In this research, the possibility of exploiting the extraordinary properties of this compound to obtain a new theranostic platform consisting of ultrasmall nanoparticle-based PB nanochains is investigated, using a process that is at the same time simple, fast and green. The study then goes on to analyse the properties of these assemblies as potential carriers. The results of the research give some initial demonstrations of the wide variety of molecules that these assemblies are able to carry, not only drugs but also dyes for their tracking during in vitro studies and NO molecules to make anti-cancer treatments even more effective.

RÉSUMÉ

Le cancer est aujourd'hui une des maladies les plus redoutées de l'humanité, nombreuses méthodes ont été conçues pour le traiter et l'imager. Dans ce contexte, le bleu de Prusse (PB) peut être utilisé dans l'application simultanée de plusieurs traitements pour obtenir un agent théranostique stable et biocompatible avec des propriétés extrêmement utiles et intéressantes. Sa structure poreuse et chargée électriquement en fait un support possible pour l'administration de médicaments; sa capacité à absorber le rayonnement proche infrarouge (NIR) en fait un agent pour les traitements photothermiques (PTT). En même temps, le PB est aussi un excellent agent de contraste pour diverses techniques d'imagerie, comme l'imagerie photoacoustique (PAI) ou l'imagerie par résonance magnétique nucléaire (IRM), qui peuvent être utilisées en même temps de manière double.

Dans cette recherche, on étudie la possibilité d'exploiter les propriétés extraordinaires de ce composé pour obtenir une nouvelle plateforme théranostique composée de nanochaînes PB à base de nanoparticules ultrafines, en utilisant un procédé à la fois simple, rapide et vert. L'étude se poursuit par l'analyse des propriétés de ces assemblages en tant que porteurs potentiels. Les résultats de la recherche donnent quelques premières démonstrations de la grande variété de molécules que ces assemblages sont capables de transporter, non seulement des médicaments mais aussi des colorants pour leur suivi lors d'études in vitro et des molécules de NO pour rendre les traitements anticancéreux encore plus efficaces.

ACKNOWLEDGEMENTS

First of all, I want to thank my supervisor Laure Catala who has always helped and supported me despite all the problems we have both encountered over the past few months, a special thanks goes to Riya George, without her constant help and valuable advice much of the work that is presented here would probably not be there.

I want to thank warmly my family, my dad, my mum, my brother and especially my grandfather for all the support, all the warmth and especially all the patience they have had with me, I would not be here without them.

A huge thank you goes to Luigi, for inspiring me in my studies and always supporting me in my research without ever doubting my chances

I would also like to thank all those who have given me joy and serenity over these years, be they human, non-human, inanimate objects or state entities, thanks to Maddalena, Bianca, Eloisa, Guido, Herbert, Michele, Dr. Michael Morbius, Jean-Pierre (written like this), Gabriele, Lucas, the Most Serene Republic of San Marino, Guido, Figaro, Joe Kruppetto, Serena, Jeanne, Antonello and Ilaria.

I want to thank the SERP+ project and all those who help to keep it going, most notably Eva and Kali. Thank you for this wonderful experience.

I think I also owe a special thanks to Pacaterie, thank you for making me a stronger person and helping me to improve both my physical and mental endurance.

Finally, the biggest thanks goes to *BUONASERA*, thank you very much my friends for all the beautiful and unforgettable moments we experienced together.

This work is dedicated to all of you.

"Muchas gracias afición esto es para vosotros: SIUUUU" (Ronaldo C.)

LIST OF ABBREVIATIONS

5FU – penta-fluorouracil

CA – contrast agent

DDS – drug delivery system

DLS – dynamic light scattering

EPR – enhanced permeation and retention

GA – Gallic acid

MRI – magnetic resonance imaging

NIR – near infrared radiation

NP – nanoparticles

PA – photothermal agent

PAI – photoacoustic imaging

PB – Prussian blue

PTT – photothermal treatment

SNP – sodium nitroprusside

TEM – transmission electron microscopy

1. INTRODUCTION

Cancer is one of the diseases that we inevitably carry with us from the dawn of time. Numerous attempts have been made in the past to seek cures for this ailment: Egyptian, Greek and Roman doctors, among others, tried to treat this disease[1]. However, it was only with the emergence of modern medicine that we finally had a clear idea of what a tumour was and thus tried to develop effective treatments.

Cancer is a plague on our modern society (fig.1): the numbers show that the number of patients is constantly increasing and that it can affect any person regardless of origin, gender or age[2]. This scourge is not only human and social, but also causes enormous economic damage to our society, forcing it to invest numerous resources in its fight. It has been calculated that in 2010 alone, the cost incurred by the world economy due to cancer was USD 1.16 trillion[3]. Despite this immense expenditure, however, the prevalence of cancer shows no sign of abating and, as the world's population increases, the number of people with cancer is also estimated to increase drastically , causing immense pain and death(fig.2)[4].

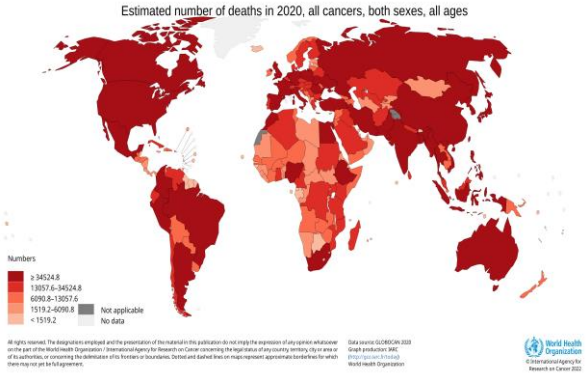

Figure 1- Deaths caused by cancer in 2020 – ref. in the image

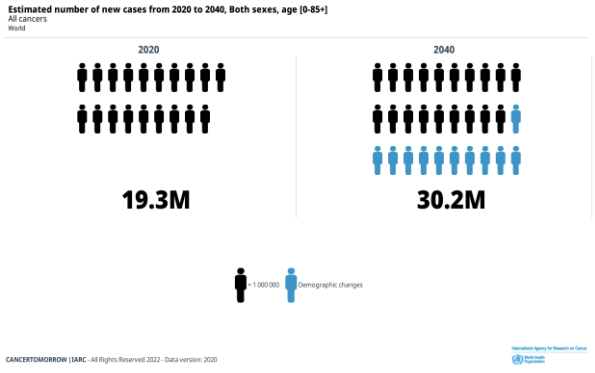

Figure 2-Estimated increase in cancer patients from 2020 to 2040 – ref. in the image

Nowadays numerous treatments have been developed to treat cancer patients, and they range from simple surgery to advanced treatments involving the use of stem cells. All these treatments are a necessity because cancer can potentially affect any person and it is important then to develop an adaptable and personalized form of treatment depending on the patient. The most commonly used form of treatment is chemotherapy, where drugs are used to stop or slow down the growth of cancer cells[3]. However, they can indiscriminately effect healthy tissues in the body and cause harmful side effects including, among the others, intense fatigue, sores on mouth, nausea and hair loss[5]. To limit the adverse effects and provide better quality of life to patients, it is essential to optimize the amount of drug applied and get maximum-targeted therapy. Hence, drug delivery systems (DDS) have been a highly focused area of research.

1.1 Drug Delivery Systems

DDSs help to transport the medication specifically to the area of the body where the problem to be treated is present. By minimizing the diffusion of drug molecules throughout the human body, a higher efficiency of the treatment can be achieved and most of the unpleasant side effects could be avoided[6]. In addition to the medical factor, there is also an economic advantage. Developing a new

pharmaceutical treatment is a slow, difficult and expensive process, while designing a new DDS would cost only 10% of the amount[7]. Drug delivery systems could be broadly classified into two main types, depending on their targeting strategies.

1.1.1 Passive targeting

The passive targeting is based on the so-called Enhanced permeability and retention effect (EPR effect, fig.3), theorised by Matsumura and Maeda in 1986[8]. According to them, due to the typical fast development of tumour cells, a strong stimulus for the generation of new vasculature near the tumour site is generated. These new blood vessels, because of the rapidity of their generation, show numerous abnormalities compared to the normal blood vessels. They are disorganized, permeable and leaky which is advantageous in designing a treatment strategy. The gaps within the vessels (figure 4) are of nanometres scale and hence 50-150 nm sized particles or macromolecular drugs can easily pass through and enter the cancerous tissues[6,9]. The poor lymphatic drainage from the tumour leads to its retention for an extended period, making nanoparticles an ideal drug delivery system[10]. However, particles with sizes over 100 nm are easily recognized by macrophages within the body and tend to accumulate in organs like the liver, spleen, lungs and lymph nodes[11]. This accumulation could lead to possible complication and it is important that the large NPs be cleared out of the body after the treatment is done[12]. On the other hand, the ultra-small sub-10 nm particles would be rapidly cleared by the kidney through the renal excretion system due to the pore size of the filtration system[13]. This very fast clearance also limits the therapeutic efficiency and so it is highly essential to control the size of nanoparticles used for bio-medical purposes.

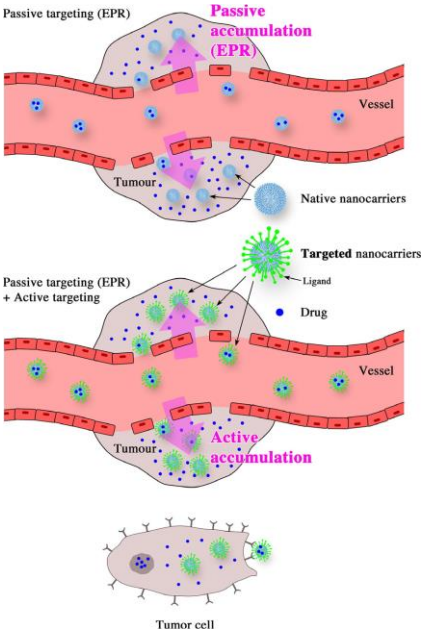

Figure 3 - Passive targeting and active targeting [14]

1.1.2 Active targeting

It should be pointed out that the passive targeting strategy is rather simple and is based solely on the ability of the carrier to remain 'trapped' within the tumour clusters. As it does not rely on specific interactions between the carrier and the tumour cells, only a 20-30% increase in drug transport compared to healthy organs can be obtained[14]. This limitation can be overcome by active targeting, in which case one relies not only on the EPR effect but also on the functionalisation of the surface of the nano-carrier to specifically transport molecules to the region of interest[11]. We will not dwell on this strategy any further in this report, as it goes beyond the scope of the performed internship. However, it can be considered as a possible future extension, given the ease with which the assemblies described here can be functionalised. At present, the development of DDSs is a field in full expansion (fig.4). In recent

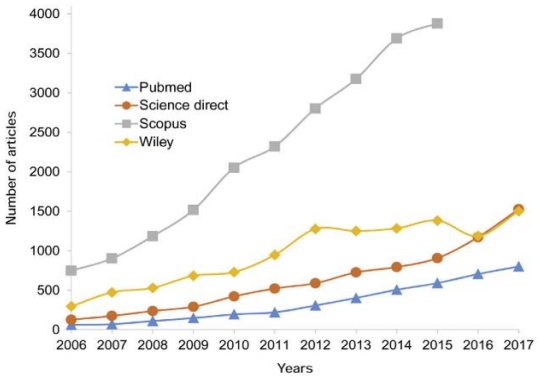

Figure 4 - The increase of interest for DDSs over the years: published articles with the keywords "nanoparticle and drug delivery" [12]

years, more and more research has been carried out in this field[12], and numerous carriers with very different characteristics have been developed. This project is focussed on Prussian blue nanoparticles, which has all the characteristics to become one of the most promising DDS.

1.2 Prussian blue and its uses

Prussian blue (PB) is a chemical compound that has been known for more than three centuries. It is the first modern synthetic pigment, discovered by German artist Johann Diesbach in the early 18th century[15]. It is a coordination compound, with a face-centred cubic structure in which Fe^{2+} and Fe^{3+} ions are linked via cyanide bridges in the following way: Fe^{2+}–C≡N–Fe^{3+}(Figure 7)[16]. The intense blue colour characteristic to Prussian blue is derived from intervalence band due to the metal-to-metal charge transfer between Fe^{II} and Fe^{III} [17].

Prussian blue can exist in two forms (fig.5)[16]:

- Insoluble: $Fe^{III}_4[Fe^{II}(CN_6)]_3 \cdot xH_2O$ (x=14-16)
- Soluble: $KFe^{III}[Fe^{II}(CN_6)] \cdot xH_2O$ (x=1-5)

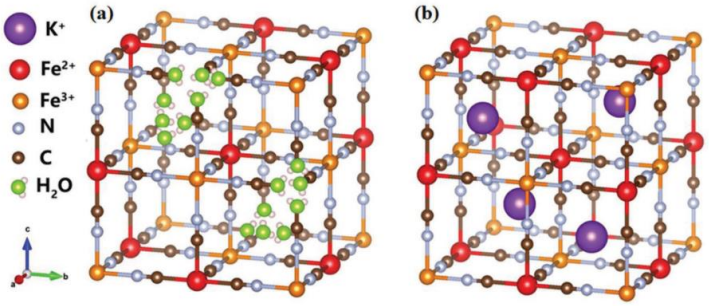

Figure 5 - PB unit cell: a) insoluble PB; b) soluble PB [16]

The soluble PB gives rise to a stable colloidal dispersion in water. This is due to the inclusion of K^+ ions in its structure, which dissociate giving PB structure an overall negative charge[18].

The most commonly used method to obtain the PB nanoparticles is coprecipitation: it takes place between a salt of Fe^{3+} with $K_4[Fe(CN)_6]$, but in practice the opposite can also be done, i.e. reacting a salt of Fe2 with $K_3[Fe(CN)_6]$[19]. Once the two solutions have been mixed it can be observed the immediate appearance of the classic blue colour due to the charge transfer present in the complex. It is important to note that both soluble and insoluble PB can be obtained with this reaction, and the stoichiometric ratio between the two reagents plays an important role in determining the final composition. If the two reagents are equimolar then soluble PB will be synthesised, whereas when the iron salt is in excess then insoluble PB is the form that will prevail[17].

Over the last few years, this compound has attracted increasing interest for its potential applications in the field of nanoscience (magnetism, batteries…)[20]. Here, we will concentrate only on the - albeit numerous - properties that can be used in the biomedical field. One of the reasons behind the great interest of PB in scientific research lies in its ability to be used for many different scopes at the same time, for both diagnostics and therapy, thus making it a theranostic agent. The reason for this versatility lies in some of its physical characteristics[16,18,21]:

- Its strong stability due to the high formation constant
- It has a porous structure that allows it to accommodate molecules and ions
- it has a strong absorption band in near infrared radiation (NIR)

It should be noted in fact that at present, PB has already been approved in 2003 by the U.S. Food and Drug Administration (FDA) to treat radioactive from thallium and caesium ions[22]. Moreover, its green and low-cost synthesis without any surfactants is an additional advantage. Its imaging and therapeutic use will be summarized below.

1.2.1 Imaging

PB is a valuable contrast agent (CA) in a variety of different imaging techniques, and its practicality allows it to be used with several techniques at the same time, often complementary to each other.

Magnetic resonance imaging (MRI) represents one of the most powerful imaging techniques available to medicine with an excellent spatial resolution: it uses powerful magnetic fields that interact with the nuclear spins of the water hydrogen atoms in our bodies. Depending on the environment in which the nuclei of the atoms are located, the longitudinal (T1) and transverse (T2) relaxation times of the nuclei will be different; the whole process of reconstructing the image of the body by the computer is based on this difference. Some exogenous CAs based on paramagnetic ions are introduced to shorten the relaxation times. Gd(III) chelates are commercial T1-CAs that lead to positive contrast (brightening), but are subject to debate due to some toxicity issues[23].

In this context, Prussian blue is a good candidate as highly stable and based on iron ions. It has been shown that sub-20 nm PB particles acts as T1-CA due to the presence of the paramagnetic Fe^{3+} ions with exchangeable water molecules[24].

In addition to MRI, the PB can also be used for photoacoustic imaging (PAI) a technique that relies on the properties of certain materials to absorb radiation and release the absorbed energy via sound waves[25]. The use of PB as a contrast agent (CA) in this technique (due to his good absorption in the IR), enables the replacement of other CAs such as gold nanostructures or carbon nanotubes that cost considerably more and have unknown long-term toxicity [25,26].

By exploiting the many properties of PB at the same time, it is possible to achieve what is called multimodal imaging, i.e. an image acquisition using PB as the CA of several different techniques[27].

1.2.2 Photothermal treatment

Photothermal therapy (PTT) is a treatment strategy that induces cell death by heating the cancerous tissues, this technique relies on the ability of specific wavelengths of the infrared electromagnetic spectrum to penetrate easily the human body, which between 600 and 1300 nm (in the so called biological window) is almost transparent to radiation[28]. A photothermal agent (PAs) has to absorb the electromagnetic radiation and to re-emit the energy in the form of heat. PB is an excellent PTT agent, due to its strong absorption band in the biological window[29].

The first use of PB as a PTT agent was demonstrated in 2012[30], since then there have been numerous researches using PB as a PA. However, the main limitations of this technique is that it often fails to eradicate the tumour completely[29]. Therefore using it in combination with other techniques, such as chemotherapy prove extremely beneficial[31].

1.2.3 Combined therapy

At present, a great number of research studies have been published on the use of PB as drug carriers for combined therapies. Yu and Wang designed hollow mesoporous PB nanoparticles that can encapsulate doxorubicin (DOX)[32], a potent anti-cancer drug with a high encapsulation efficiency. Stimuli-responsive release of the loaded compounds could be achieved and the ability of PB to heat the local environment further enhances the drug release. They have successfully shown that the two treatment techniques work synergistically to improve the overall therapeutic efficiency.

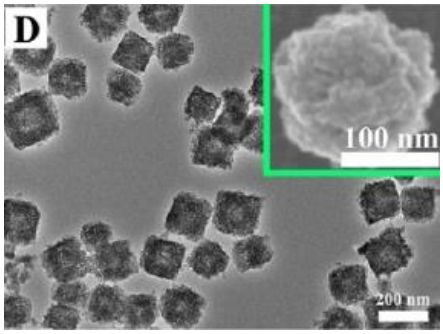

Figure 6 - Example of hollow mesoporous PB NPs [32]

However, these PB structures are larger than 100 nm (fig.6) in size and there is a high probability of its accumulation in the body. Furthermore, chemical etching is used to create the porosities within the PB[32], employing harsh conditions that deviate from what should be the green chemistry principles of environmental sustainability in reactions: use of aqueous solvents and mild reaction conditions[33].

The use of PB as a carrier can also be extended to other categories of molecules other than anticancer drugs: Feng, Wan *et al.* published a paper in 2019 in which they highlight the ability of PB also as a carrier of NO, always in the perspective of developing anticancer treatments[34]. In their study, they exploited the similarity between the chemical structure of potassium ferricyanate and sodium nitroprusside (SNP) (fig.7) to insert NO inclusions within its crystal structure during the synthesis of PB. This allowed them to obtain NPs of 100 nm in diameter in which NO could be released following laser irradiation in the NIR. The release of NO into the cellular environment has important consequences since, when dosed appropriately, it induces neighbouring cells to undergo apoptosis[35]. This study therefore opens up to the possibility of introducing a new functionality to PB-based NPs, in addition to the already described PTT, imaging, and drug delivery. The major application obstacle of the NPs just described, similar to the other NPs described above, lies in their large size, which makes them an easy target for the human body's defence mechanisms.

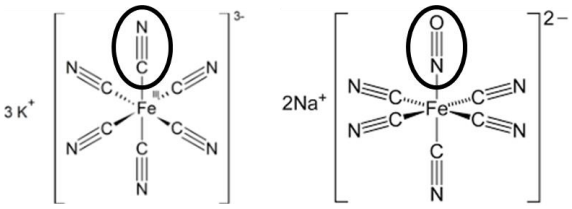

Figure 7 - The similarity between ferricyanate and nitroprusside

By using PB as DDS is possible then to obtain a theranostic nanoplatform, where the sole use of NIR light allow to combine several different properties:

- The stimuli-responsive release of the loaded compounds (drugs or NO)
- The heating due to the photothermal effect
- Imaging due to the photoacoustic effect
- T_1 contrast imaging in MRI due to the presence of Fe^{3+}

The research carried out in this placement moves precisely in this direction; the following section provides a brief theoretical description of the project under development that may be helpful in understanding why the assemblies studied here may be of great interest and usefulness.

1.3 Aim of the work: theranostic PB-based nanochains

The aim of this research is to further study self-assemblies made from PB ultrasmall NPs. The size of PB NPs is finely tuned through a low-temperature reaction and fast addition, which allows controlled nucleation by reaching a high supersaturation to obtain PB NPs with a size below 10 nm[26].

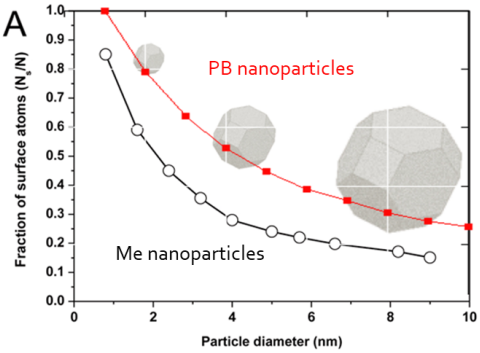

Figure 8 - Change of the proportion of atoms on the surface with the NPs size

Working with such small NPs offers the advantage of having a better contrast effect in MRI: the smaller the diameter of a particle, the greater the ratio of its surface area to its volume, (fig.8) this allows for a greater proportion of Fe^{3+} atoms on the surface compared to larger structures and therefore the contrast effect is increased. Moreover, in the microporous PB structure, it leads to about 50% of atoms for a crystal size of 5 nm. All water molecules coordinated on the surface will be very efficient for affecting T1 relaxation time.

However, single ultrasmall PB NPs do not yet constitute an ideal carrier for drug transport. In order to have greater accumulation of PB in the tumour site, encapsulate drugs with a high payload onto it, and increase the residence time in the human body, it is necessary for these NPs to be assembled to form larger structures. It has been found that in the presence of Gallic acid, a polyphenolic ligand with a strong affinity for Fe^{3+} ions[36], PB NPs assemble to form linear one-dimensional chains. This form can be explained, as illustrated in previous cases involving gold NPs[37,38], by considering the DLVO theory, which explains the aggregation processes of nanoparticles in an aqueous environment. According to the theory, the potential energy for chain formation derives from two opposing contributions: the attractive Van der Waals forces and electrostatic repulsion. In the present case, a change in the ionic strength of the reaction environment can cause a change in the local electrostatic force, which is no longer homogeneous but changes in intensity if it is at one end of the chains or at their side, thus favouring the formation of linear nanochains.

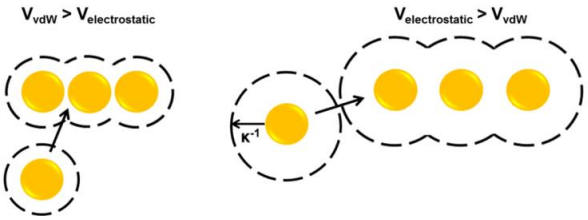

Figure 9 - How the change of the electrostatic force influences the chain formation [38]

Moreover, further advantages given by the nature of these self-assemblies, formed by a union of several NPs are:

- A better contrast for MRI (fig. 10), as each individual NPs adds its contribution to the others in the chain

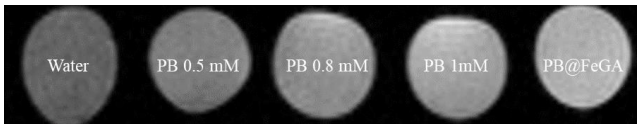

Figure 10 - Phantom images at 9.4T of the MRI contrast effect

- The possibility, in the event of chain breakage at the end of treatment, of easy elimination of the PB by renal cleansing, given the small size of the constituent NPs.

Regarding the properties of PB@FeGA as a drug carrier studied by our group, the results obtained with doxorubicin by Riya George as part of her PhD are noteworthy: these assemblies posses an encapsulation efficiency of 96.2% and a payload of 36.6%, using DOX with a concentration of 47uM. This research project has been developed on three different directions, all focused on improving the potential of the nanochains as vector for the drug delivery and they are as follows:

- Reproducing the previous results and loading new drugs

- Using fluorescent dyes for tracking the assemblies during *in vitro* studies
- Studying the NO release from the nanochains

The first part is aimed at studying the reproducibility of the PB@FeGA synthesis process, and to expand the range of possible drugs that can be loaded onto them. Doxorubicin possesses a global positive charge, and by exploiting the electrostatic interactions with the (negatively charged) assemblies, and formation of H-bonds with the PB's CN groups, a high drug encapsulation could be acheived. The study of loading other drugs such as penta-fluorouracil (5-FU), a neutral molecule, makes it possible to understand whether interactions via H-bridges alone are sufficient for effective loading.

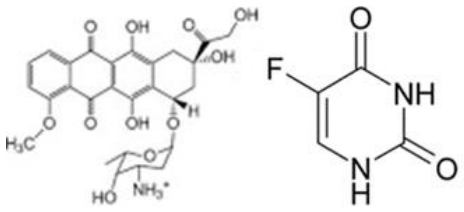

Figure 11 - DOX (left) and 5-FU (right)

The use of a fluorescent dye, in this case 7-hydroxy coumarin (from now on only coumarin), allows, in the case of successful loading, the chains to be easily traced during *in vitro* studies of the process of chain internalisation in cells. Since coumarin is also neutral, the study would add information on the behaviour of such molecules in addition to that provided by 5-FU.

The possibility of inserting NO within the utrasmall NPs of PB and to trigger its release would make it possible to create a new type of assemblies with the properties of NPs described in the previous section but without the disadvantage of large size, thus being able to be used without the risk of being accumulated within the body.

2. MATERIALS AND METHODS

2.1 Materials

All the starting materials were obtained from commercial suppliers and used without further purification:

Ferric nitrate ($Fe(NO_3)_3 \cdot 9H_2O$); potassium ferrocyanide ($K_4[Fe(CN_6)] \cdot 3H_2O$), Gallic acid (GA), poly gamma cyclodextrin citrate (γCD-Cit.), sodium nitroprusside ($Na_2[Fe(CN_5)NO] \cdot 2H_2O$), 7-hydroxy coumarin, 5-fluorouracil 5-FU and doxorubicin (DOX)

The ultrafiltration tubes, purchased from Vivaspin, used have a membrane with two different pore sizes: 5000 Da and 300000 Da.

Ultrapure milli-Q (18.2 $M\Omega \cdot cm^{-1}$) and distilled water were used as the only solvent during the entire study.

2.2 Synthesis

One of the strengths of the assemblies on which this thesis is based is their easy and green synthesis. The scheme illustrated below provides a summary of the work. The realisation of these nano-chains is fast, involves only a few steps in water and is easily achievable even in laboratories without sophisticated equipment.

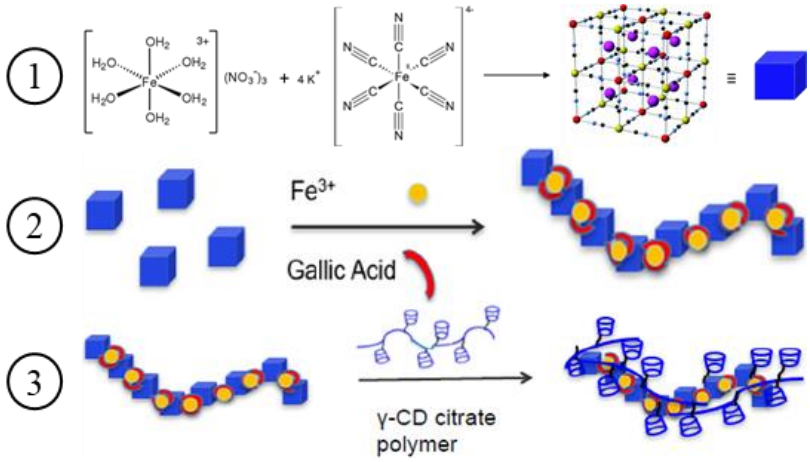

Figure 12 – The synthetic process of PB@FeGA

It consists of 3steps:

1. The synthesis of Prussian blue
2. The formation of nano-chains
3. The polymer coating

Each of these steps will now be properly described here in this section.

2.2.1 The synthesis of Prussian blue

Prussian blue is obtained through a co-precipitation reaction involving two salts: ferric nitrate and potassium ferrocyanide, the synthesis takes place by quickly adding an equimolar solution of ferric nitrate to a 0.5 mM solution of ferrocyanide, keeping the solution shielded from light and under constant stirring for 30 minutes, the final expected concentration of PB is 0.25mM. This reaction takes place in an aqueous environment at a temperature of 2°C, controlled by means of a thermostatically controlled ice bath. It is essential that the temperature remains constant during the reaction in order to obtain homogenous NPs of the desired size.

Once the reaction is complete, the resulting PB must be kept away from light at all times, as it is photosensitive. To ensure that the reaction is carried out correctly, the size of the NPs obtained can be approximated using DLS.

2.2.2 The formation of the nanochains

The next step is the construction of the actual nanochains, using the PB synthesised in the previous step as building blocks. Gallic acid (GA) is a polyphenol with a high affinity for Fe^{3+}. The systematic addition of the reagents into pre-formed PB facilitates assembly formation; the final product is labelled as PB@FeGA.

The two reagents are prepared by solubilising ferric nitrate and Gallic acid, having first neutralised it by addition of dilute $NaOH_{aq}$ controlled with a pH-meter. The synthesis procedure involves dropwise addition of two solutions of Fe^{3+} (8 mL, 0.5mM = 2 Eq.) and GA (8 mL, 1 mM = 4 Eq.) at the rate of 0.5 mL/min using a peristaltic pump to the PB solution (8mL, 0.25 mM) and under constant stirring.

Once the addition is complete, the solution is left to react for 30 minutes before the stirring is stopped. The final expected concentration of PB in the nanochains is 0.083 mM. DLS measurements are used to get an indication of the approximate size of the obtained nano-chains.

2.2.3 The polymer coating

The third step is the addition of a polymer coating with a dual function: improving the stability of the chains and increasing the effectiveness of drug loading. The polymer chosen for this dual task is poly-γ cyclodextrin citrate (γCD-Cit.), synthesised by the group of Ruxandra Gref (ISMO). The solution containing the nanochains (50 mL, 0.083mM) is added to the aqueous solution containing the polymer (50 mL, 4.15μM = 0.05 Eq.). The solution is then kept under constant stirring for 30 minutes and, after that, it undergoes a purification step to remove the excess not bound to the chains. The obtained product (PBFeGA + γCD-Cit.) is expected to have a concentration of 0.0415mM.

The purification step involves ultrafiltration (UF). Using Vivaspin tubes that have pores with an average diameter of 5000 Da, ensures that the unreacted species and salts filter out, while the nano-chains remain at the top. The UF step involves the filtration of 15 mL of solution in three (one filtration + two sample washes) centrifugation cycles (speed 6000 rpm for 15 min at room temperature). At the end of each cycle, the supernatant is brought back to its original volume with water.

2.3 Further experiments

2.3.1 The loading

The polymer has been chosen initially to entrap DOX in the CD cages, but indeed other interactions can take place between the drug and chains as discussed later. For the actual conditions of the individual experiments, see the section "Results and analysis".

Water-soluble drugs have been chosen and are introduced in the nanochains solution. At the end of the set time, the dispersion is then purified by separating the uncharged part from the assemblies containing the compound by means of ultrafiltration, in which case 5,000 or 300,000 kDa ultrafiltration tubes can be used depending on the type of experiment.

2.3.2 Release experiments

Once the substance has been loaded onto the assemblies, it is necessary to study the conditions under which it can be released in order to understand the applicability of the chains in future treatments. First, the reaction environment is no longer exclusively aqueous, so to simulate the cellular environment, the release is studied in the presence of foetal bovine serum (FBS). Furthermore, to simulate the neutral pH of the blood a phosphate buffered saline (PBS, pH 7.4) was used.

The solution in which the release is studied is prepared as follows: first FBS (10% of the final volume) is added to the chains (50% of the final volume), and then the buffer (40% of the final volume) is added under stirring. In parallel, a control sample is also prepared by adding just water to the assemblies. The release study is carried out by preparing several samples, examined at different times. Each sample, before undergoing spectrography, is ultrafiltered to remove the released part of the loaded compound.

2.3.3 PB with NO inclusions

The preparation of PB with inclusions of NO within the crystal structure constitutes a variant of the method described so far for the synthesis of assemblies. It involves the addition of sodium nitroprusside (SNP). Two preparation strategies to prepare the PB-NP have been attempted, the results of which will be discussed in the appropriate chapter.

1st method: starting with the building blocks

Following the example given in the literature[34], and discussed in the introduction, an attempt was made to create a PB with SNPs from the basic components, i.e. iron (III) ions, potassium ferrocyanide and sodium nitroprusside. Two solutions were then prepared, one containing only Fe^{3+} (in the same concentration as that prepared for the normal synthesis of PB, 0.5mM) and a second solution containing nitroprusside and ferrocyanide in varying proportions (see the "results and analysis" section), prepared in turn from two stock solutions of SNP and potassium ferrocyanate. Once the two solutions have been prepared, the procedure is identical to that described for the synthesis of PB: Fe^{3+} is added to the mixture of SNP and potassium ferrocyanide under stirring and at 2°C, and left to react for 30 minutes, again in a darkened bottle for protection from light.

2nd method: starting from PB

Another experimented method involves adding SNPs to the pre-formed PB dispersion, leaving the SNP to react with the PB surface for 1 hour and 30 minutes under agitation. The reaction conditions including concentrations and volumes of reagents were optimized to obtain stable self-standing nanoparticles in water.

2.3.4 NO detection

A Griess assay kit (Sigma Aldrich) was used to determine the NO released during heating. The determination is based on the use of two reagents, Griess Reagent I, to reduce any nitrate present to nitric oxide, and Griess Reagent II, which forms with NO a stable pink dye that allows the determination with colorimetry by measuring its absorbance at 450 nm. The kit used contained the two Griess reagents and the necessary to prepare standard solutions of nitrite for the calibration curve.

The samples for the essay were prepared in the following way:

200 µL of sample + 60 µL of nitrite assay Buffer + 40 µL of Griess reagent 1 + 40 µL of Griess reagent 2 + 60 µL of nitrite assay buffer

2.4 Characterisation

Transmission electron microscopy

The images obtained with the transmission electron microscope were obtained in the CNRS *"Institute for Integrative Biology of the Cell (I2BC)"* laboratory in Gif-sur-Yvette. TEM JEOL microscopes at 80 and 120 kV were used for the studies. The sample preparation consists of the deposition of 100 µL on formvar coated copper grids from Agar Scientific previously glow discharged with a PELCO easyGLow and left to air dry a few minutes.

Dynamic light scattering and zeta potential

A Malvern Zetasizer with backscattering mode instrument was used both for DLS measurements and to obtain the zeta potential. This type of measurement requires approximately 1 mL of sample.

IR spectroscopy

In this study, the IR spectra were obtained using a Perkin Elmer spectrum 100. To prepare the sample for measurement, it is precipitated by adding a saturated NaCl solution, allowed to settle overnight and then centrifuged at low temperature. Once the supernatant solution has been removed, the remainder is dried under vacuum. Finally, approximately 1 mg of the product is combined with 99 mg of anhydrous potassium bromide, ground and pressed to form a pellet for the measurement.

UV-VIS spectroscopy

UV-VIS spectra were obtained using a Cary Win UV 5 spectrophotometer, with 3mL quartz cuvettes.

Fluorescence spectroscopy

An Agilent Cary Eclipse fluorescence spectrometer was used for experiments involving 7-hydroxy coumarin: 30uL of solution are put in a quartz cuvette, filled until 3 mL with water (100-fold dilution is necessary because of the intense dye signal).

3. RESULTS AND ANALYSIS

3.1 Loading of drugs and nanochains

3.1.1 Reproduction of the assemblies and first *in vitro* results

As mentioned in the introduction to this section, the reproducibility of previously obtained results was verified. The steps described in the assembly synthesis section were then replicated and the synthesised product was characterised by UV-VIS spectroscopy, DLS, zetametry and lastly TEM.

UV-VIS spectroscopy

The first comparison is absorption in the NIR region, which is important for future applications in PA imaging and PTT. The initial PB NPs and the nanochains obtained at the end of the process are compared (fig.13) with the ones obtained by Riya George, the PhD student who developed the synthesis process to assess the correct reproduction of the method.

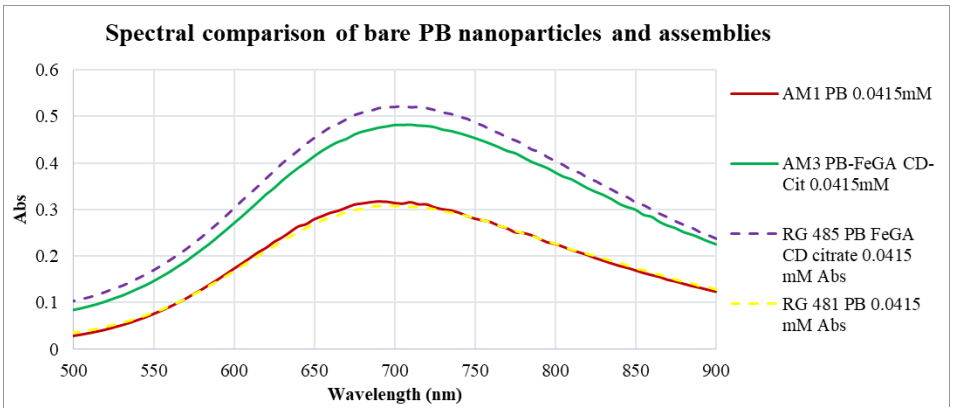

Figure 13 - Comparison between different synthetic results

The molar attenuation coefficient ε [$L \cdot mmol^{-1} \cdot cm^{-1}$] calculated at 710 nm for the four samples is:

Table 1 - The obtained molar attenuation coefficients

Sample	*Andrea MERLO*	*Riya GEORGE*
PB	7.7	7.5
PB-assemblies	11.6	12.5

Both the shape and intensity of the peaks are approximately the same, providing initial evidence of the reproducibility of the experiment. The higher intensity of the chains compared to the NPs alone should be noted; this is due to the formation of the complex called iron gallate (FeGA) during synthesis, which shows a strong absorption in the NIR region

DLS and zetametry

Table 2 - The DLS/zetametry characterisation results

Sample	***Hydrodynamic diameter [nm]***	***Zeta potential [mV]***
PB	7.68 ± 2.12	-12.9 ± 8.6
PB-assemblies	80.67 ± 31.17	-26.7 ± 5.5
PB-assemblies with polymer	64.83 ±37.63	-28.6 ± 5.2

It can be seen that the synthesis yields negatively charged NPs, as stated in the introduction. It should also be noted that the addition of the polymer leads to a further increase in absolute value of the zeta potential, thus contributing to improved stability of the assemblies.

TEM

Ultra-small PB of 5.4±0.9 nm size were synthesised. As shown in fig.14, assemblies of these nanoparticles PBFeGA with an average size of 62.5 ± 18.8 nm were formed. It can be seen that the formed assemblies retain the same shape even after the addition of the polymer and ultrafiltration.

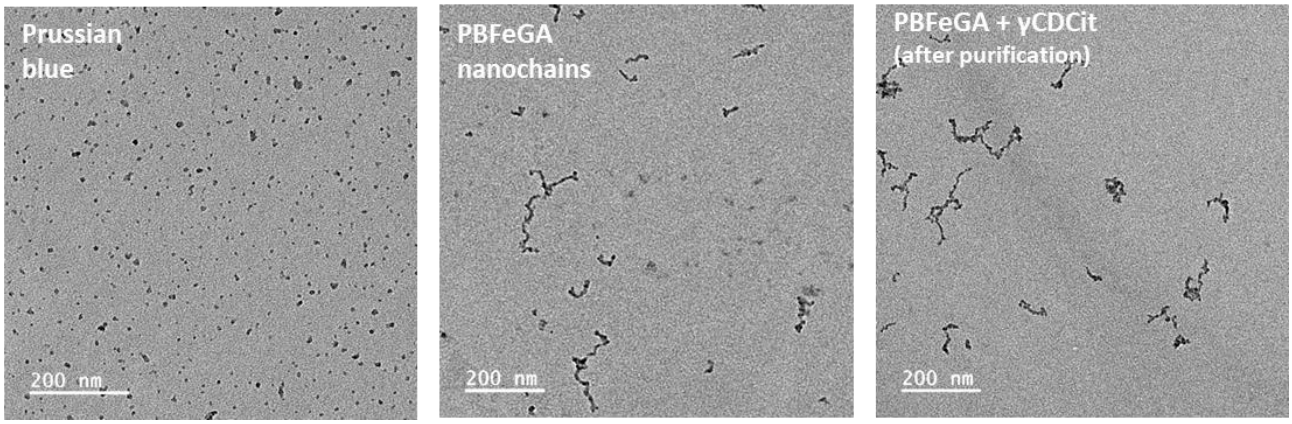

Figure 14 - TEM images of the different steps in the synthetic process

After this comparison of the various results obtained from the characterisation techniques, the process can be considered as reproducible and capable of providing a stable colloidal suspension of nano-chains, thus suitable for use in an in vitro assay on cell cultures, after loading the drug, DOX.

DOX loading and *in vitro* experiment

Drug loading was carried out by adding DOX (47 uM) to PBFeGA + γCD-Cit ultrafiltrated assemblies (41.5 uM). The samples were incubated for one hour, in the dark at room temperature before purification by UF using the 300-kDa tubes. The loading efficiency could be studied by UV-Visible spectroscopy and the samples were sent to Grenoble for *in-vitro* studies. The experiments were carried out in IAB, Université Grenoble-Alpes by our collaborator Prof. Lucie Sancey. The following images show the results obtained through fluorescence measurements using a confocal microscope on human cancer cell samples of the U87-MG type.

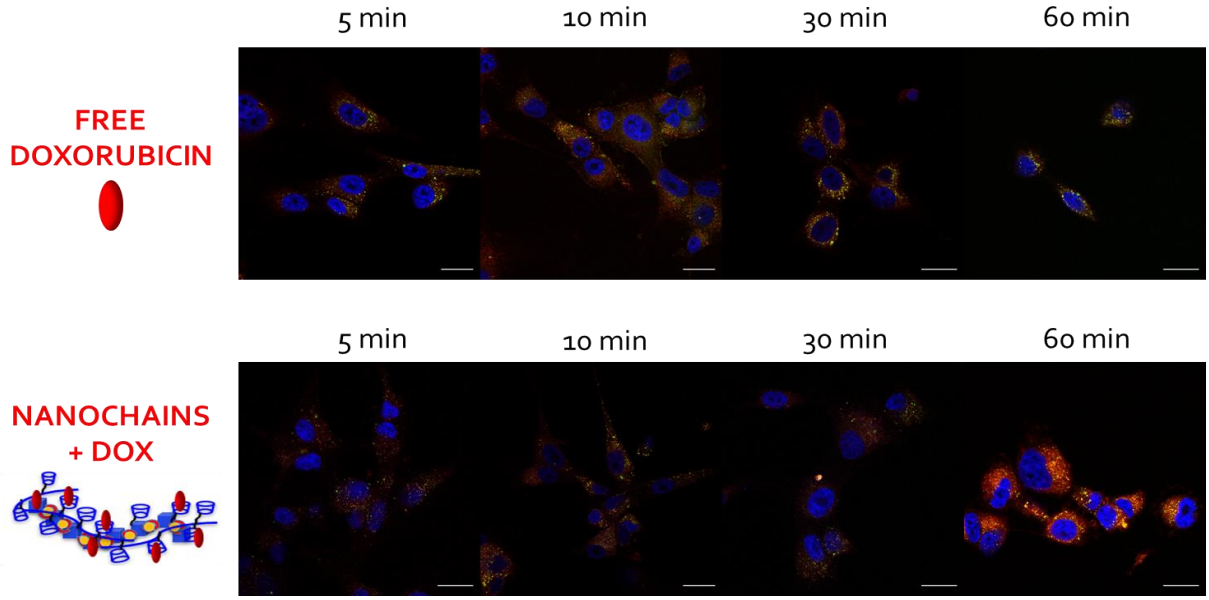

Figure 15 - Comparison of the change of fluorescence with time coming from free DOX and DOX loaded on the assemblies

This first study (fig.15) compares the internalisation of DOX when it is free in the extracellular environment with the case when it is loaded onto the assemblies. It can be clearly seen that within 1 hour after administration the drug bounded to the nanochains is well internalized in the cells resulting in the increase of fluorescence whereas the free Dox shows much less inclusion. This study therefore offers proof of the potential of the assemblies as a means of transporting DOX inside cells; however, it does not provide any evidence on the internalisation of the chains inside the cells. The chains alone are not fluorescent and the fluorescence coming from the DOX trapped on the chains is quenched, and only when the drug is released (after 60 minutes) is possible to observe the phenomenon.

The need to be able to follow the pathway of assemblies during *in vitro* administration is one of the reasons for the set of fluorescence experiments described in second section of this chapter.

3.1.2 Loading neutral molecules on the PB@FeGA: attempts with fluorouracil

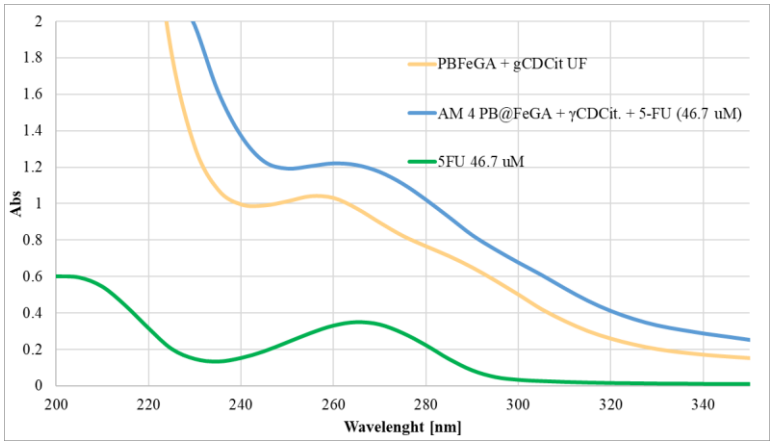

Figure 16 - Superimposition of the 5FU signal and the assemblies signal in the UV region

What was obtained from DOX loading bodes well for the potential of assemblies as transport carriers, however, these results are based on two factors, previously discussed, both of which contribute to the results obtained: electrostatic chain/drug attraction and hydrogen bonds chain/drug and polymer/drug. In order to get an idea of the relative contribution of the two effects, they need to be evaluated separately. In particular, it is of great importance to evaluate the contribution given by hydrogen bonds in the loading, as this would make it possible to extend the range of molecules that can be loaded onto the chains to include neutral molecules as well,

and not only cationic molecules such as DOX. The experiments carried out with penta-fluorouracil (5-FU) are therefore aimed at this purpose, however a precise determination of the loading of 5-FU was impeded by the superimposed signal in the UV-visible spectrum (fig.16) of 5-FU and PB@FeGA assemblies. HPLC separation would be needed and we preferred to switch to a fluorescent molecule 7-hydroxycoumarin. Indeed, it is of great importance in *in vitro* studies to have techniques for monitoring the uptake in cells. One of the simplest and most effective techniques is undoubtedly fluorescence spectroscopy.

3.2 Loading of 7-hydroxycoumarin

Ideally, this dye (fig.17) if loaded on the assemblies could allow their tracking during *in vitro* experiments, and plus, since it can create hydrogen bonds similarly to the 5-FU, in a release study it could give an idea of what could be the behaviour of such neutral drug.

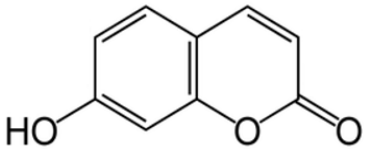

Figure 17 - Chemical structure of 7-hydroxycoumarin

The first step consists of loading dye onto the assemblies: a coumarin stock solution is added to the solution containing the assemblies with polymer coating and the final concentration of the added dye is 50 uM.

The emission spectrum presented here (fig.18, λ_{ex} = 335 nm) shows the variation of the signal obtained from coumarin with time.

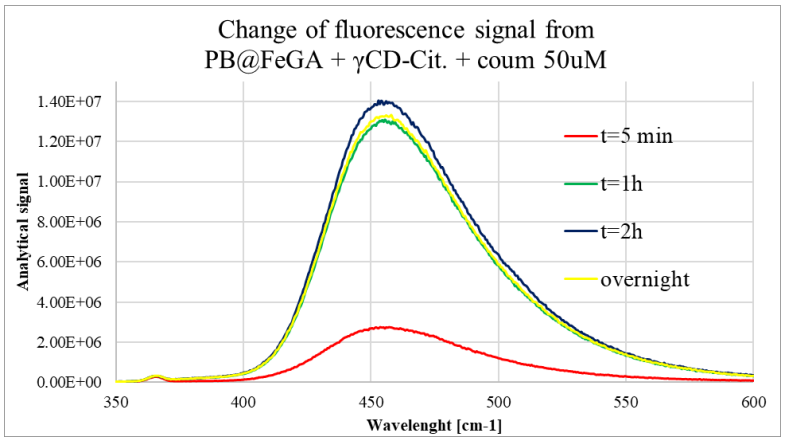

Figure 18 - Change in fluorescence signal with time of assemblies loaded with coumarin

Table 3 - Change in the coumarin concentration in solution with the assemblies over the time

Assemblies with polymer + coum. 50µM	**Coumarin detected [uM]**
t = 5 min	13.2
t = 1h	54.5
t = 2h	58.5
Overnight	55.5

It can be noticed that at the beginning, there is a quenching of the signal, however after a short time, this phenomenon stops and the signal becomes strong and stable for a long time. A possible explanation for this phenomenon could be that the dye immediately after addition may initially form aggregates, thus limiting its ability to excite, when the molecules disperse in solution this effect disappears and fluorescence is observed.

The table 3 shows the coumarin concentration values obtained by means of a calibration curve and it shows that concentration value obtained is in line with what was calculated. The result establishes that there is no quenching of the fluorescence, apart from the brief initial quenching phenomenon. This is an improvement on previous studies carried out with DOX by our group, as the drug loaded onto the chains, as opposed to coumarin, does not fluoresce, thus making it impossible to trace the chains, as described in the previous section.

The next step was the UF purification of the solution to remove the excess coumarin not loaded on the assemblies; the graph 19 shows the signal before and after the process, using the tubes with pore limit of 300 kDa. This step presented considerable criticality, as with both 5 kDa and 300 kDa tubes, coumarin tends to be stuck in the pores, making it difficult to quantify the exact amount of coumarin actually loaded in the nano-chains, since the amount of coumarin left in the pores or in the filtrate cannot be determined.

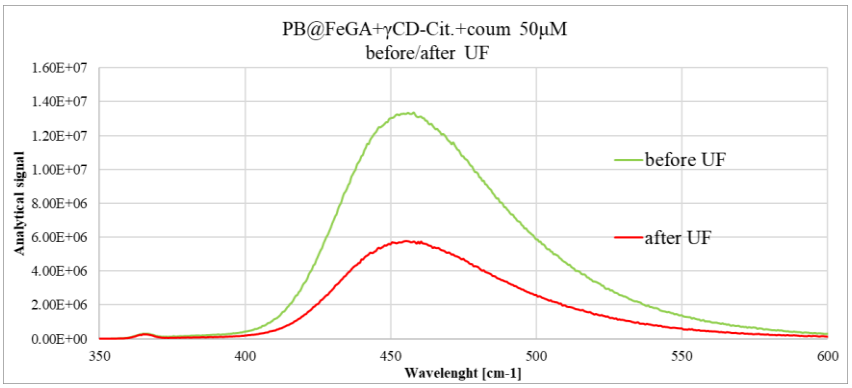

Figure 19 - Change in fluorescence of assemblies loaded with coumarin before and after ultrafiltration

Table 4 - Change in the coumarin concentration in solution before and after ultrafiltration

Sample	Coumarin conc. [uM]
Before UF	55.5
After UF	25.1

Still it can be assumed that the remaining signal present in top part of the tube after the process is attributable to coumarin loaded in the chains only. So we can conclude that 45.2% of encapsulation efficiency (EE) is obtained, which gives a weight loading around 9.5%

The next step is the coumarin release study:

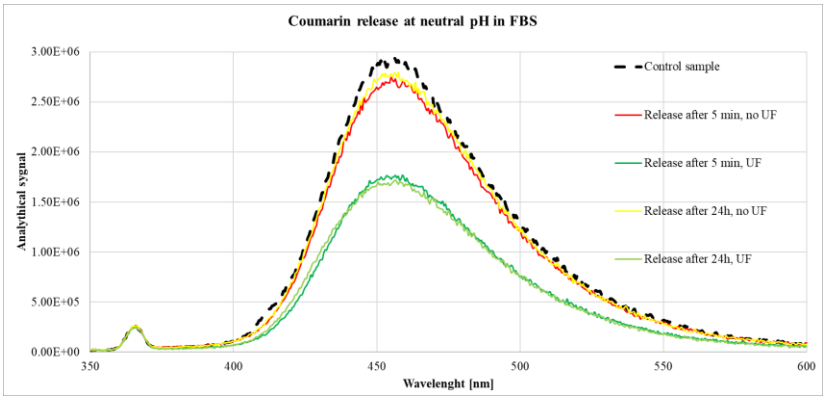

Figure 20 - Coumarin release with time at neutral pH in a biological environment

Table 5 - Coumarin released from the assemblies at neutral pH in FBS with time

Sample	Coumarin conc. [uM]
Control sample	13.8
t = 5 min before UF	13.1
t = 5 min after UF	9.3
t = 24 h before UF	13.3
t = 24 h after UF	9.1

The release was performed in the presence of FBS to simulate the biological environment and neutral pH of 7.4 was maintained using PBS buffer. Samples were analysed at different time points to understand the mechanism of release. Ultrafiltration was done to remove the released coumarin and fluorescence measurements indicated the amount remaining bound to the PB chains. Calibration curve was used to determine the exact concentration and results obtained are displayed in table 5. Results of intermediate time points have been omitted for the sake of simplicity. The graph and table show that coumarin release at neutral pH is independent of time, and the comparison with the control test shows that it is not environment-dependent. Several interesting results were obtained from this experiment:

- It is possible to load neutral molecules onto the chains effectively (EE = 45%) by relying only on the hydrogen bridges between the dye and the assemblies.

- The fluorescence of coumarin, unlike that of DOX, remains in the chains, making it possible to track them in in vitro experiments.
- There is a burst release of around 29% of the dye after only 5 minutes at neutral pH, which could cause problems for *in vivo* tracking applications. However, after this time the concentration remains stable indicating that the rest of coumarin is strongly bonded to the nanoassemblies.
- For future experiments using other neutral molecules, the H-bonds formed are strong enough to guarantee loading, however the aim is to minimise the initial release.

3.3 Nanochains for combined NO release therapy and PTT

The assemblies investigated in this study have so far been examined as carriers for the transport of drugs; however, the transport can also be extended to other categories of molecules useful in fighting cancer. As mentioned in the introduction, therapy based on gas release and especially of nitric oxide is of interest. Our goal was to introduce sodium nitroprusside in the ultrasmall PB NPs, as SNP has five cyanide groups that can coordinate to Fe^{3+}.

First objective: the synthesis of the PB-NP

Two strategies were attempted to obtain PB-SNP. One involves the direct synthesis from PB constituents (Fe^{3+} and $[Fe(CN)_6]^{4-}$) mixed with SNP, while the second involves the addition of SNP to the already formed PB leading to a grafting at the surface. In both cases several ratios of PB:SNP were used trying to find a stable dispersion while minimizing the dilution of NP that may affect later the nanochains formation.

Table 6 - Summary of all the samples prepared with PB and SNP

Experiments staring from basic constituents	**Experiments starting from pre-formed PB**
Fe^{3+} + $[Fe(CN)_6]^{4-}$ + SNP (1:1:12) Precipitated	PB:SNP (1:1) Unstable
Fe^{3+} + $[Fe(CN)_6]^{4-}$ + SNP (1:1:0.5) Unstable	PB:SNP (1:6) DLS: 8.9±2.1 nm
Fe^{3+} + $[Fe(CN)_6]^{4-}$ + SNP (1:0.9:0.1) Unstable	PB:SNP (1:8) DLS: 10.5±2.9 nm
Fe^{3+} + $[Fe(CN)_6]^{4-}$+ SNP (1:0.5:0.5) Precipitated	PB: SNP (1:10) DLS: 10.8±3.1 nm
	PB:SNP (1:12) DLS: 9.4±2.5 nm
	PB: SNP (1:14) Unstable

These attempts in many cases yielded poor results as the dispersions either precipitated shortly afterwards or were too unstable to be relied upon following zeta potential measures. As expected for simple grafting on preformed PB particles allows obtaining stable dispersions, while on the other hand the formation of PB-SNP starting from the precursors is quite problematic.

Among the stable dispersion obtained, the PB-SNP (1:12), due to the higher content of SNP; is the most suitable one to move forward with the next steps, from the characterisation presented here it seems similar to the regular PB in size, shape and absorption, moreover it possess also a good stability (-33.8±9.1 mV).

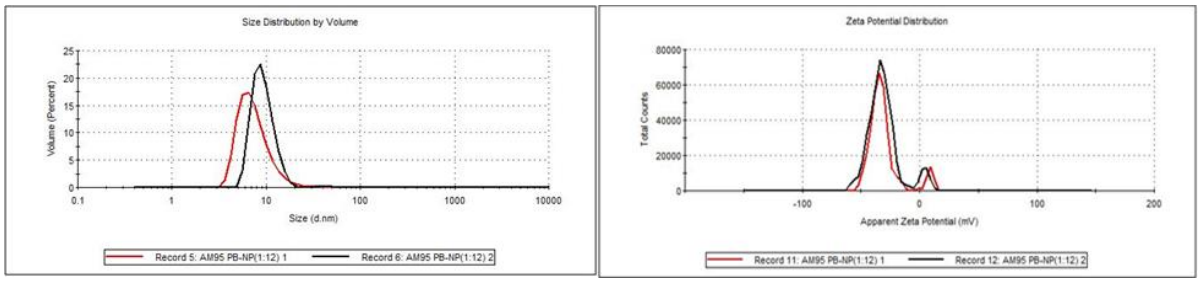

Figure 21 - DLS and zeta potential graphs from PB-SNP (1:12)

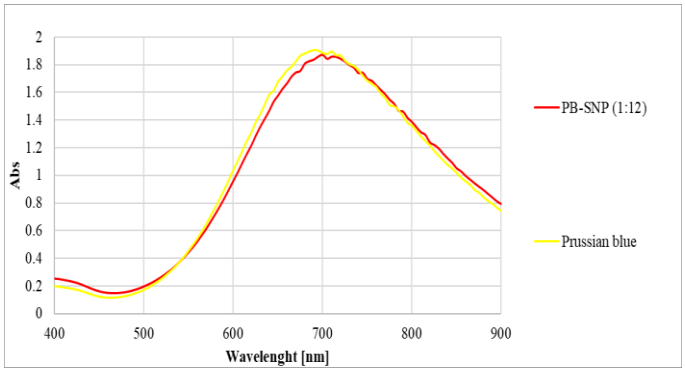

Figure 22 - UV comparison of normal PB and PB-SNP(1:12)

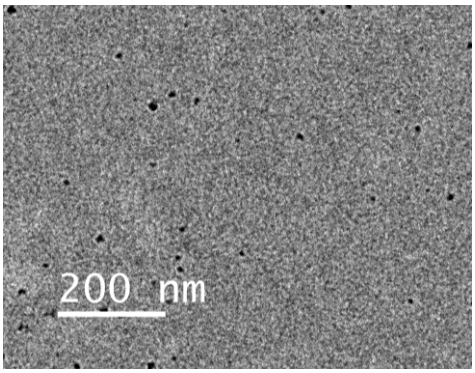

Figure 23 - TEM image of PB-SNP(1:12)

With all the previous characterization, it is not possible to prove the presence of NO within the NPs. To do this, the dispersion containing PB-NP (1:12) was first ultrafiltered to remove excess unreacted SNP from the solution. The PB nanoparticles were then recovered as powders by addition of a saturated salt solution (see materials and methods) and then examined by FTIR spectroscopy (fig.24). The objective of the measurement is to verify the presence of the vibrational band of the N=O bond present at 1944 cm^{-1}. The graph shows the results obtained with both PB-NP (1:12) and PB-NP (1:6).

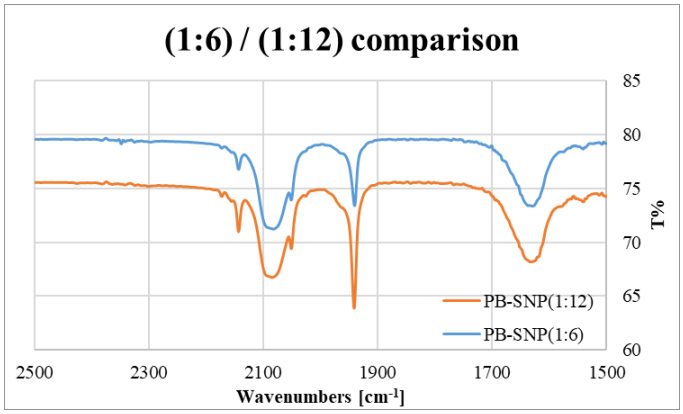

Figure 24 - IR comparison of PB-SNP(1:12) and PB-SNP(1:6)

The IR spectrum confirms the presence of NO within the PB-NP. An increase in the intensity of the NO band is proportionate to the nitroprusside added in the dispersion, proving that the amount of NO present is tunable by adjusting the amount of precursor used. Moreover, it is also possible to observe the band coming from the stretching of the CN groups at 2086 cm^{-1} and at 1632 cm^{-1} the one generated by the bending of the OH groups present in the water included in the PB crystal structure.

Second objective: the assemblies

The next step is to obtain, similarly to what is done with normal PB, nanochains using Fe^{3+} and GA. In this sections are reported the results obtained using PB-NP (1:12) nanoparticles which, as shown in the previous section, are the most promising NPs obtained.

DLS, zetametry, UV-VIS / FTIR spectroscopy and TEM were performed. From the data provided on it can be observed that the size, stability, shape and absorption spectra appear similar to that of normal PB@FeGA. However, IR spectroscopy suggests that the actual NO content is extremely low compared to the initial PB/SNP particles (see fig.27).

It was assumed that the dilution during the synthesis (the PB-SNP is diluted by a factor of three) might have led to dissociation of some nitroprusside. Therefore, new assemblies were synthesised, in this case using higher concentrations (1mM and 2 mM of Fe^{3+} and GA respectively) therefore reducing the dilution factor from three to two. Other attempts were made with even more concentrated solutions, however, resulting in unstable dispersions that deposited quickly.

The results obtained from DLS, zetametry, TEM and UV-VIS and FTIR spectroscopy are as follows.

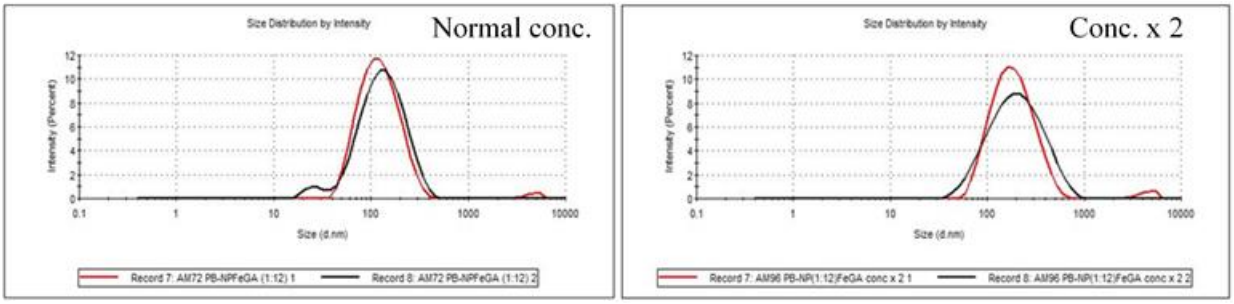

Figure 25 - DLS comparison of the two types of PB-SNP(1:12)@FeGA

Table 7 - DLS and zeta potential results for the two types of PB-SNP(1:12)@FeGA and normal PB@FeGA

Sample	*Hydrodynamic diameter [nm]*	*Zeta potential [mV]*
PB@FeGA	80.67 ± 31.17	-26.7 ± 5.5
PB-SNP(1:12)@FeGA with normal conc of reagents	88.9 ± 50.3	-33.8 ± 9.1
PB-SNP(1:12)@FeGA with double conc. of reagents	200.9 ± 100.1	-34.7 ± 4.6

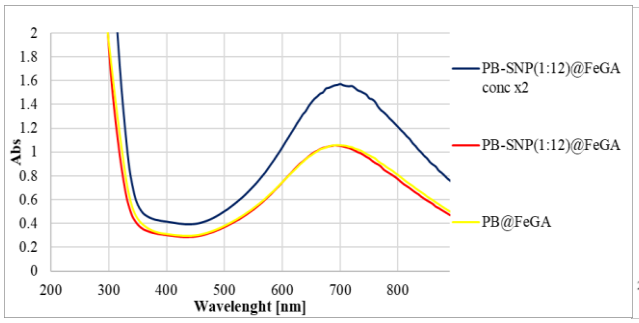

Figure 26 - UV-VIS spectra of the two types of PB-SNP(1:12)@FeGA and normal PB@FeGA

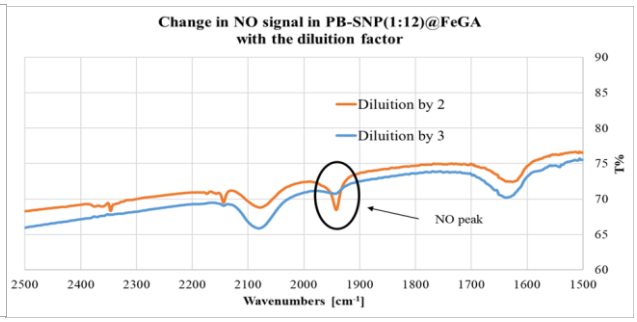

Figure 27 - Effect of the dilution on the IR NO peak in the PB-SNP(1:12)@FeGA

These new nanochains show similar features in DLS, zeta potential and TEM (with apparently longer nanochains, see table 7). Still there are two main differences compared to the chains synthesised using the standard conditions:

- The first concerns the UV-VIS spectrum, which shows a more intense peak in the NIR, probably due to the formation of additional PB bridges when adding the iron gallate complex, thus increasing absorption at those wavelengths.
- The second is the presence of a more pronounced NO peak than previously obtained, showing that the lower dilution helped in increasing the intensity of this signal.

Now that both NPs and potentially useful assemblies for NO transport have been prepared, the next section deals with experiments to verify the release of the gas in the case of heating, as is the case in the article mentioned above[34].

Third objective: the release of NO

In this section, the qualitative results on NO release from PB-NP (1:12) and PB-NP (1:12)@FeGA are briefly presented. The heating of the dispersion by IR laser is simulated by heating the two solutions in a flask under reflux at 70°C for 1 hour. Once the heating is complete, the presence of NO is detected using the Griess method, as low amounts cannot be detected by IR spectroscopy.

The NO that is released is transformed to nitrite and nitrate that reacts to form an azo compound as explained in the Materials and Methods section. By using a calibration curve with standards, it is possible to determine the concentrations of NO released by the sample.
The results have been studied at neutral and acidic pH on both the starting NPs and assemblies and are summarized in the table 8.

Table 8 - NO release from bare PB-SNP(1:12) NPs and PB-SNP(1:12)@FeGA

Sample	**Conc. NO released [µM]**
NPs alone	2.7
NPs + 1h heating	18.5
NPs + ac. buffer	7.1
NPs + ac. buffer + 1h heating	22.5
Assemblies alone	0
Assemblies + 1h heating	1.5
Assemblies + ac. buffer	0.8
Assemblies + ac. buffer + 1h heating	8.8

Many interesting results were obtained from this experiment:

- Firstly, both NPs and assemblies are able to release NO when heated, so the main aim of the experiment was achieved.
- In addition, it can be seen that in the presence of an acidic environment, and with heating, the release of NO is even more pronounced, thus making the release of NO in the presence of tumours even more efficient.

However, it should be noted that the release of NO from the assemblies is less than that from the NPs; one hypothesis to explain this behaviour may be due to the capping effect of FeGA, which would

prevent release. However, even if the amount released from the chains is rather small, it may still be sufficient to induce a decrease in tumour mass, as proven in the literature[34].

Unfortunately, due to the lack of sufficient time to investigate adequately this phenomenon, the results obtained cannot be considered exhaustive; the only certain experimental evidence is that it is possible to stimulate the release of NO through heating. How this release occurs and what parameters are used to control it is not yet known, so further experiments will be needed to answer these questions.

CONCLUSIONS AND PERSPECTIVES

A number of different experiments have been carried out in this internship, a brief summary of which will now be given here with some comments.

With regard to the nanochains, the confirmation of the ease with which these can be produced and functionalised is an important result that gives hope for a possible extension of the synthesis process on a larger scale. With this in mind, as a future perspective, an important goal to be achieved is to be able to fine-tune their size, just as it was possible to do for PB NPs. This could be achieved by microfluidics techniques or Size Exclusion Chromatography.

Concerning the ability of these assemblies to carry neutral molecules, the results with 5-fluorouracile were not concluding even if the absorption spectra showed apparently the grafting. Ultracentrifugation should be used in the future to quantitatively determine the loading. A better result, which gives a better idea of the strength with which neutral molecules can bind to chains only using hydrogen bonds, was obtained with coumarin. Despite the major problems related to the retention of much of the dye in the pores of the UF tubes during purification, an encapsulation efficiency of 45.2% was obtained after 24 hours and a loading estimated around 9.5%. These results will be replicated in the following months. It can be seen that the release study at pH=7.4 shows that there is a stable concentration of coumarin loaded onto the assemblies and that it is able to provide a clear analytical signal, even if a burst release occurs after 5 minutes. A further attempt, which is still in progress, is to first load only a small amount of coumarin, only 10% of the assemblies, which is more than enough for tracking, and only after the dye-loading, coat the whole thing with the polymer, to try to trap better the dye, this release will be studied soon. Indeed, we want the dye to be strongly maintained on the nanoassemblies in order to track them during in vitro studies by FLIM of their internalisation, in order to understand the corresponding mechanism.

Finally, the results obtained with sodium nitroprusside, to investigate the possibility of increase the range of treatments that can be used with our assemblies, gave excellent preliminary results. It has been demonstrated that it is possible to insert NP within the PB structure and that it is possible to achieve NO release from both the nanoparticles and the assemblies, even if the mechanism has not yet been fully understood. The NO will be quantified by elemental analysis on the starting NP. The important point that has to be checked is the efficiency under an 808 nm laser. Indeed, it is well known that the local heating provoked at the vicinity of the PTT nanostructures gives rise to a much higher local increase of temperature that is not equivalent to the average temperature of the medium. We expect that in nanoassemblies this effect can be collective and improve the NO release activated by PTT. This will be checked *in vitro* by comparing standard assemblies to NO-containing assemblies under NIR-irradiation of the wells.

REFERENCES

1. Cancer: A Historic Perspective | SEER Training. Accessed June 22, 2022. https://training.seer.cancer.gov/disease/history/

2. Cancer Today. Accessed June 22, 2022. https://gco.iarc.fr/today/online-analysis-map?v=2020&mode=population&mode_population=continents&population=900&populations=900&key=total&sex=0&cancer=39&type=1&statistic=5&prevalence=0&population_group=0&ages_group%5B%5D=0&ages_group%5B%5D=17&nb_items=10&

3. Cancer. Accessed June 22, 2022. https://www.who.int/health-topics/cancer#tab=tab_1

4. Cancer Tomorrow. Accessed June 22, 2022. https://gco.iarc.fr/tomorrow/en

5. Side Effects of Cancer Treatment > Fact Sheets > Yale Medicine. Accessed July 14, 2022. https://www.yalemedicine.org/conditions/side-effects-cancer-treatment

6. Allen TM, Cullis PR. Drug Delivery Systems: Entering the Mainstream. *Science (80-).* 2004;303(5665):1818-1822. doi:10.1126/science.1095833

7. Wouters OJ, McKee M, Luyten J. Estimated Research and Development Investment Needed to Bring a New Medicine to Market, 2009-2018. *JAMA - J Am Med Assoc*. 2020;323(9):844-853. doi:10.1001/jama.2020.1166

8. Matsumura Y, Maeda H. A New Concept for Macromolecular Therapeutics in Cancer Chemotherapy: Mechanism of Tumoritropic Accumulation of Proteins and the Antitumor Agent Smancs. *Cancer Res*. 1986;46(8):6387-6392.

9. Lavik EB, Kuppermann BD, Humayun MS. Drug Delivery. In: *Retina Fifth Edition*. Vol 1. Fifth Edit. Elsevier Inc.; 2012:734-745. doi:10.1016/B978-1-4557-0737-9.00038-2

10. Ranade V V., Hollinger MA. *Drug Delivery Systems*.; 2003. doi:10.9774/gleaf.9781315302317-14

11. Wu J. The enhanced permeability and retention (Epr) effect: The significance of the concept and methods to enhance its application. *J Pers Med*. 2021;11(8). doi:10.3390/jpm11080771

12. Simonazzi A, Cid AG, Villegas M, Romero AI, Palma SD, Bermúdez JM. Nanotechnology applications in drug controlled release. In: *Drug Targeting and Stimuli Sensitive Drug Delivery Systems*. ; 2018:81-116. doi:10.1016/B978-0-12-813689-8.00003-3

13. Han Y, Park K. Targeted drug delivery to tumors : Myths , reality and possibility. *J Control Release*. 2011;153(3):198-205. doi:10.1016/j.jconrel.2011.06.001

14. Attia MF, Anton N, Wallyn J, Omran Z, Vandamme TF. An overview of active and passive targeting strategies to improve the nanocarriers efficiency to tumour sites. *J Pharm Pharmacol*. 2019;71(8):1185-1198. doi:10.1111/jphp.13098

15. Ware M. Prussian blue: Artists' pigment and chemists' sponge. *J Chem Educ*. 2008;85(5). doi:10.1021/ed085p612

16. Busquets MA, Estelrich J. Prussian blue nanoparticles: synthesis, surface modification, and biomedical applications. *Drug Discov Today*. 2020;25(8):1431-1443. doi:10.1016/j.drudis.2020.05.014

17. Samain L, Grandjean F, Long GJ, Martinetto P, Bordet P, Strivay D. Relationship between the synthesis of Prussian blue pigments, their color, physical properties, and their behavior in paint layers. *J Phys Chem C*. 2013;117(19):9693-9712. doi:10.1021/jp3111327

18. Qin Z, Li Y, Gu N. Progress in Applications of Prussian Blue Nanoparticles in Biomedicine. *Adv Healthc Mater*. 2018;7(20):1-13. doi:10.1002/adhm.201800347

19. Uemura T, Kitagawa S. Prussian blue nanoparticles protected by poly(vinylpyrrolidone). *J Am Chem Soc*. 2003;125(26):7814-7815. doi:10.1021/ja0356582

20. Chiang YH. Research and Application of Prussian Blue in Modern Science. In: *IOP Conference Series: Earth and Environmental Science*. Vol 384. ; 2019. doi:10.1088/1755-1315/384/1/012005

21. Dacarro G, Taglietti A, Pallavicini P. Prussian blue nanoparticles as a versatile photothermal tool. *Molecules*.

2018;23(6):1-20. doi:10.3390/molecules23061414

22. Busquets MA, Novella-Xicoy A, Guzmán V, Estelrich J. Facile synthesis of novel Prussian blue-lipid nanocomplexes. *Molecules*. 2019;24(22):4137. doi:10.3390/molecules24224137

23. MRI scan - NHS. Accessed July 14, 2022. https://www.nhs.uk/conditions/mri-scan/

24. Shokouhimehr M, Soehnlen ES, Hao J, et al. Dual purpose Prussian blue nanoparticles for cellular imaging and drug delivery: a new generation of T1-weighted MRI contrast and small molecule delivery agents. *J Mater Chem*. 2010;20(25):5251-5259. doi:10.1039/B923184F

25. Qin Z, Li Y, Gu N. Progress in Applications of Prussian Blue Nanoparticles in Biomedicine. *Adv Healthc Mater*. 2018;7(20):1800347. doi:10.1002/adhm.201800347

26. Fétiveau L, Paul G, Nicolas-Boluda A, et al. Tailored ultra-small Prussian blue-based nanoparticles for MRI imaging and combined photothermal/photoacoustic theranostics. *Chem Commun*. 2019;55(98):14844-14847. doi:10.1039/c9cc07116d

27. Lee N, Yoo D, Ling D, Cho MH, Hyeon T, Cheon J. Iron Oxide Based Nanoparticles for Multimodal Imaging and Magnetoresponsive Therapy. *Chem Rev*. 2015;115(19):10637-10689. doi:10.1021/acs.chemrev.5b00112

28. Lee C, Jeon M, Kim C. Photoacoustic imaging in nanomedicine. *Appl Nanosci Photomed*. Published online January 1, 2015:31-47. doi:10.1533/9781908818782.31

29. Estelrich J, Antònia Busquets M. Iron oxide nanoparticles in photothermal therapy. *Molecules*. 2018;23(7):1567. doi:10.3390/molecules23071567

30. Fu G, Liu W, Feng S, Yue X. Prussian blue nanoparticles operate as a new generation of photothermal ablation agents for cancer therapy. *Chem Commun*. 2012;48(94):11567-11569. doi:10.1039/C2CC36456E

31. Chen H, Ma Y, Wang X, Wu X, Zha Z. Facile synthesis of Prussian blue nanoparticles as pH-responsive drug carriers for combined photothermal-chemo treatment of cancer. *RSC Adv*. 2017;7(1):248-255. doi:10.1039/c6ra24979e

32. Yu B, Wang C. Tunable Synthesis of Mesoporous Prussian Blue@Calcium Phosphate Nanoparticles for Synergic Chemo-Photothermal Cancer Therapy. *ChemistrySelect*. 2020;5(35):10841-10847. doi:10.1002/slct.202001234

33. Basics of Green Chemistry | US EPA. United States Environmental Protection Agency. Published 2022. Accessed July 14, 2022. https://www.epa.gov/greenchemistry/basics-green-chemistry#twelve

34. Feng T, Wan J, Li P, et al. A novel NIR-controlled NO release of sodium nitroprusside-doped Prussian blue nanoparticle for synergistic tumor treatment. *Biomaterials*. 2019;214(May). doi:10.1016/j.biomaterials.2019.05.024

35. Fan W, Yung BC, Chen X. Stimuli-Responsive NO Release for On-Demand Gas-Sensitized Synergistic Cancer Therapy. *Angew Chemie - Int Ed*. 2018;57(28):8383-8394. doi:10.1002/anie.201800594

36. Ponce A, Brostoff LB, Gibbons SK, et al. Elucidation of the Fe(III) Gallate Structure in Historical Iron Gall Ink. *Anal Chem*. 2016;88(10):5152-5158. doi:10.1021/acs.analchem.6b00088

37. Stover RJ, Moaseri E, Gourisankar SP, et al. Formation of Small Gold Nanoparticle Chains with High NIR Extinction through Bridging with Calcium Ions. *Langmuir*. 2016;32(4):1127-1138. doi:10.1021/acs.langmuir.5b03639

38. Zhang H, Wang D. Controlling the growth of charged-nanoparticle chains through interparticle electrostatic repulsion. *Angew Chemie - Int Ed*. 2008;47(21):3984-3987. doi:10.1002/anie.200705537